Available online at www.sciencedirect.com
SCIENCE DIRECT®
International Journal of Multiphase Flow 31 (2005) 53–68
International Journal of Multiphase Flow
www.elsevier.com/locate/ijmulflow

Hydrodynamically interacting droplets at small Reynolds numbers

W. Holländer [a], S.K. Zaripov [b,*]

[a] Fraunhofer Institute Toxikologie und Experimentelle Medizin, Nikolai-Fuchs-Str. 1, D-30625 Hannover, Germany
[b] Kazan State University, Institute of Mathematics and Mechanics, Universitetskaya St., 17, Kazan 420008, Russia

Received 12 February 2004; received in revised form 6 September 2004

Abstract

Droplets moving at close distances interact hydrodynamically. We present the experimental and theoretical results of a study for monodisperse 73 μm geometric diameter droplets with initial velocities between 1.5 and 3 m/s and variable generation rate (ranging from 125 to 2000 s^{-1}) emitted horizontally and vertically. During the decelerated motion the droplet Reynolds number varied between the value <1 and 10. The hydrodynamic interaction depends on the spatial distance, and we observed a considerable increase of the droplet trajectory endpoints with increasing generation rate.

Reviewing the various approaches for the description of hydrodynamic interactions, we adapted a theory for a stationary Stokes flow past a linear array of spheres and found a surprisingly good agreement between our experiments and the above model. Even better agreement was obtained by additionally taking the Basset force into account.

Keywords: Droplet interaction; Drag correction; Basset force

* Corresponding author. Tel.: +7 8432 387525.
E-mail address: shamil.zaripov@ksu.ru (S.K. Zaripov).

0301-9322/$ - see front matter © 2004 Elsevier Ltd. All rights reserved.
doi:10.1016/j.ijmultiphaseflow.2004.09.003

1. Introduction

Droplets and solid particles play an important role in many natural and industrial processes where energy, mass and momentum are exchanged between the particles. Hydrodynamic interactions, i.e. momentum exchange becomes increasingly important as the inter-particle distances become smaller which may be the case even at relatively low concentrations as they prevail in e.g. clouds, where droplet coalescence finally may lead to giant droplets falling out due to gravity.

Due to the importance of the problem much work has been carried out and still is continuously devoted to studies of the interaction of particle assemblages in various configurations.

For creeping flow, where the Reynolds number (Re) is zero, an analytical expression for the fluid velocity distribution for unbounded Stokes flows is known. Solutions to such situations were reviewed in the classical monograph of Happel and Brenner (1973). An analysis of drag change for Stokes flow past finite assemblages of particles using the multipole representation technique was presented by Gluckman et al. (1971). Within the method the disturbance due to each submerged object is represented by an infinite series of multipoles placed at the center of the object, where each multipole series has a different origin. The strength of each multipole is obtained so as to satisfy the non-slip boundary conditions along the surface of all interacting particles simultaneously. The accuracy of the method can be improved by the addition of higher order multipoles. The drag reduction results were presented for flows past chains containing up to 101 spheres.

For intermediate and high Reynolds numbers the theoretical study of particle interaction becomes more complex due to the necessity of taking into account the influence of the non-linear terms of the Navier–Stokes equations on the hydrodynamic interaction forces. Numerical approaches were used for describing the particle interactions in the non-zero Reynolds numbers regime: Tal et al. (1983), Kim et al. (1993), Raju and Sirignano (1990), Tsai and Sterling (1990), Chiang and Sirignano (1993a,b), Liang et al. (1996), among others.

Hydrodynamic interaction of particles for different configurations was studied experimentally by Rowe and Henwood (1961), Lee (1979), Tsuji et al. (1982), Nguen et al. (1991), Nguen and Dunn-Rankin (1992), Zhu et al. (1994), Liang et al. (1996), Lavergne et al. (1997), Chen and Lu (1999), and Chen and Wu (2000). The experiments of Lee (1979), Tsuji et al. (1982) pertain to the case when $Re > 125$. Rowe and Henwood (1961) measured the drag force of spherical particles in the Re number range from 32 to 96 for two aligned particles and linear chains as well as for other configurations. They found a weak Re dependence on the drag force of the trailing particle. Zhu et al. (1994) presented the results of direct measurements of the drag force on two longitudinally interacting particles for Re varying from 20 to 130. They proposed an empirical equation for the drag force variation of a single particle trailing in the wake of a leader. Liang et al. (1996) extended the experimental study of particle drag change to multiple interacting spheres of different configuration in almost the same Re range. Along with the experiments, they obtained numerical solutions to the Navier–Stokes equations for three axially aligned particles using the CFD code Fluent. Numerical drag coefficients were found to be in reasonable agreement with experiments.

Chen and Lu (1999) and Chen and Wu (2000) focused their attention on the drag and flow characteristics of a sphere in the presence of surrounding spheres of different sizes and located

at various distances and angles in a similar range of Reynolds numbers. One of the conclusions from this work is that the influence of inter-particle distance and the size of the neighbor sphere on the drag of the tested sphere increases when the neighbor sphere is located upstream of the test sphere. Fluid flow through stationary particle assemblages was also discussed in the above-mentioned works.

The influence of droplet spacing on the drag coefficient of single droplets injected into stagnant air was studied experimentally by Mulholland et al. (1988). Initial Reynolds numbers ranged from 90 to 290 and particle diameters between 205 and 450 μm. Fitting the experimental trajectories to calculated ones, they derived a formula for the drag coefficient as a function of Reynolds number and inter-particle distance.

Nguen et al. (1991) and Nguen and Dunn-Rankin (1992) presented the results of measurements and calculation of the trajectories of vertically traveling droplet packets and horizontally emitted chains of droplets. In both cases the particles (50, 127 and 145 μm) had a large initial velocity ~6–12 m/s and rapidly decelerated in still air. Again, good correlation between experiments and numerical model was observed. Under the experimental conditions the collision of a trailing droplet with the leading droplet occurred in a very short time. Because of this, the trajectory after collision of two particles was continued with one particle of combined mass. The average drag on the first trailing droplet was found to be 75% in downwards traveling packets and 90% in an initially horizontal chain.

Reviewing the literature we arrived at the conclusion that there is a gap in knowledge concerning hydrodynamic interactions in the small and intermediate region $Re < 10$ typical for cloud processes, where particle assemblages undergo the combined influence of electrostatic and acoustic forces (thunderclap) as well as hydrodynamic interaction with the latter being potentially significant in such situations.

In order to fill some gap in the above important Reynolds number range we performed an experimental and theoretical study of the decelerating motion of chains of droplets injected into still air using monodisperse droplets with a size of 73 μm varying their initial velocity between 1.5 and 3 m/s and their generation rate (generation frequency) between 125 and 2000 s^{-1}. The droplet Reynolds number is defined by $Re_p = d\rho_g|\bar{v}|/\mu$, where d is the particle diameter, ρ_g is the fluid density, μ is the fluid viscosity, $\bar{v}$ is the particle velocity vector. Using horizontal and vertical ejection directions (with respect to gravity), the droplet Reynolds number decreases from 10 to the value <1 for a deceleration of the droplet from an initial position with a constant velocity until to the droplet stopping. This Reynolds number range corresponds to the case where convective inertial effects are important but the wake behind the spherical particle has not yet formed.

In the present paper we develop a mathematical model of the quasistationary motion of droplets in a particle chain. The model takes into account the drag reduction of the particles as a function of time and inter-particle distance. The drag reduction of individual particle was found by fitting the drag correction values in stationary Stokes flow through a linear array calculated according to Gluckman et al. (1971). Comparing experimental and theoretical trajectories, the average value of drag reduction for the whole chain as a function of the droplet generation frequency was determined. The horizontal droplet trajectory endpoints and height of particle vertical jump calculated using the numerical model were compared with corresponding experimental values. The influence of the Basset force on particle chain dynamics is also briefly discussed.

2. Experimental part

The experiments were done with 73 μm geometric diameter tri-ethylene-glykole (TEG) droplets ejected horizontally (or nearly vertically) from a piezoelectric generator (Microdrop GmbH, http://www.microdrop.de) with velocities between 1.5 and 3 m/s.

The original generator was modified with a heater for operating the nozzle at constant temperature $42° \pm 0.5\,°C$ in an optimum viscosity range for stable sizes and housed (with all supporting electronics and a nozzle-imaging web camera) in a closed $5 \times 15 \times 15\,cm^3$ box providing calm air for the droplets. Trajectories of instantaneous droplet chains were photographed using a macro lens EF100 USM and a Canon EOS-D30 illuminated by a modified macro ring light MR14-EX. Intra-experiment pictures were taken at about one second intervals, and changing generation rates with precisely re-adjusting droplet speeds took about 2 min. The trajectory envelops of all experiments were highly reproducible; only the later-in-time pairwise droplet distances varied, reflecting higher order interactions (i.e. 3D trajectory curvature effects not taken into account in the 1D model) and/or slightly variable diameter/velocity initial conditions.

The stopping distance is primarily determined by the particle diameter, its density and its initial velocity. Particle diameter and velocity depend on driver voltage and pulse width applied to the piezo actuator. TEG has a density of $1455\,kg/m^3$. The geometric particle diameters g_d were determined gravimetrically from three samples of 10 000 droplets each for the individual droplet velocity and generation frequency. The results of orthogonal scans for variable generation-frequencies at constant velocity (Fig. 1a) and for variable velocity at constant generation frequency (Fig. 1b)

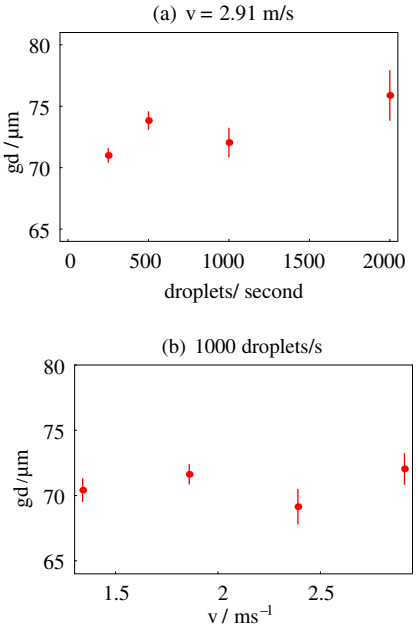

Fig. 1. Variation of geometric droplet diameter derived from gravimetry of 10 000 droplets for different generation rates and initial velocities. The error bars are one standard deviation.

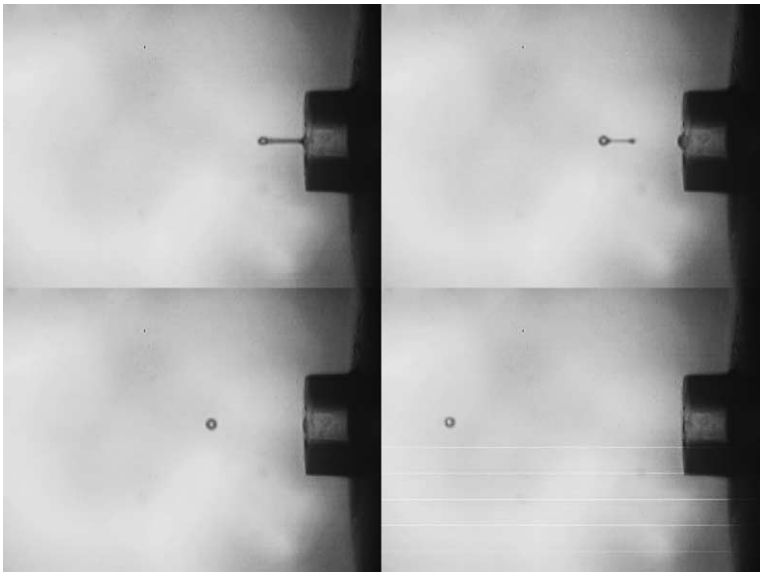

Fig. 2. Nozzle with emerging droplets after various times past the actuator pulse (118 μs: upper left; 239 μs: upper right; 298 μs: lower left; 747 μs: lower right). Frame size is $2.46 \times 1.85\,mm^2$.

are shown below. We see that the effect of changing operating conditions is reasonably small and of the order of overall gravimetric measuring uncertainty.

The initial particle velocities were determined directly at the nozzle exit from the analysis of distances travelled in certain times (see Fig. 2).

Figs. 3 and 4 show the overlay of a few typical trajectories for horizontal and nearly vertical jets, so that rising and falling droplet branches can be discriminated. The overlay was constructed

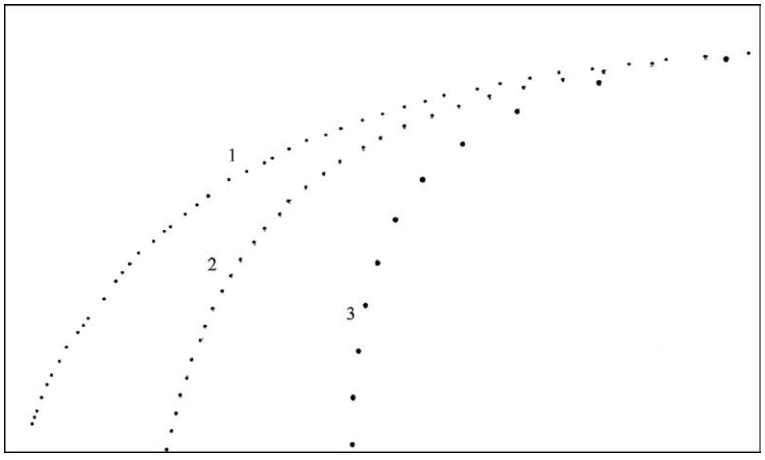

Fig. 3. Overlay of horizontal droplet jets with initial velocity of 2.39 m/s and generation rates of 160(3), 500(2) and 800(1) droplets/s (from right). Image dimension is $18.0 \times 10.8\,mm^2$.

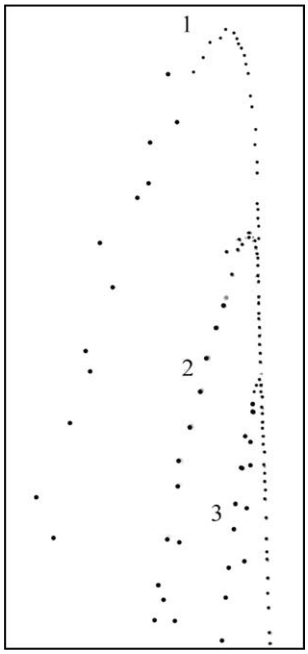

Fig. 4. Overlay of nearly vertical jets with initial velocity of 2.39 m/s and generation rates of 400(3), 1000(2) and 1600(1) droplets/s. The picture ordinate is inclined by 13° with respect to the gravity vector. Rising droplets are on the right side, where the jets overlap. Image dimension is $10.7 \times 22.7\,\mathrm{mm}^2$.

from the original JPG camera pictures by taking identical sections, converting them to a gray-scale picture, assigning the three pictures to the RGB channels and re-combining the frames to a new JPG using Mathematica 4.2 and 5.0.

3. Mathematical model formulation

Although the droplets motion is nearly two-dimensional, the experimental trajectories in the parts used for numerical calculations are smooth enough (i.e. the curvature much larger than the droplet diameter) to justify the approximation of axisymmetric flow over a sphere that is widely used to write the equation of small droplets motion. The droplets are assumed to be spherical and non-rotating. The motion of small particles in non-uniform creeping flow is described by the equation derived by Maxey and Riley (1983) (see also Michaelides, 1997). The equation of unsteady motion of a single particle for noncreeping flow is obtained by empirically modifying the Stokes law drag force and for the case of motion in still air can be written in the form (here with gravity as the only external force)

$$m_{\mathrm{p}}\frac{\mathrm{d}\bar{v}}{\mathrm{d}t} = -\frac{1}{8}C_{D0}\pi\mu d^2\bar{v}|\bar{v}| - \frac{1}{2}m_{\mathrm{g}}\frac{\mathrm{d}\bar{v}}{\mathrm{d}t} + (m_{\mathrm{p}} - m_{\mathrm{g}})\bar{g} - C_h\frac{3}{2}d^2\sqrt{\pi\mu\rho_{\mathrm{g}}}\int_0^t \frac{\mathrm{d}\bar{v}}{\mathrm{d}\tau}\frac{\mathrm{d}\tau}{\sqrt{t-\tau}}. \tag{1}$$

Here, m_p is the mass of the particle, m_g is the (in our case negligible) mass of fluid displaced by the particle and $\bar{g}$ is the gravity vector.

The first term on the right side of Eq. (1) is the stationary drag force with a semi-empirical coefficient $C_{D0}(Re)$ of the Reynolds correction of the Stokes drag law. The second term of the added mass force can be omitted due to the small ratio of the fluid density to the particle density for liquid aerosol particles in air. Next terms are the gravity and the history (Basset) forces respectively.

For the considered range of droplet Reynolds numbers we should account the deviation of the droplet drag from the Stokes drag law. Instead of the original series expansion by Oseen and others, following Clift et al. (1978), we employ the widely used empirical form of drag correction with the Reynolds number

$$C_{D0} = \frac{24}{Re_p}(1 + 0.15Re_p^{0.687}). \tag{2}$$

In our experiments we observed a decelerating motion of spherical particles in still air while, strictly speaking, particle drag coefficients could be influenced by unsteadiness. Temkin and Mehta (1982) investigated experimentally the magnitude of the departure of unsteady drag from steady one. Accordingly their results the unsteady drag coefficient in the range $9 < Re < 115$ can be expressed through the steady drag coefficient C_{D0} and the dimensionless relative acceleration parameter A by the fitting formula

$$C_{Dt} = C_{D0} - kA \quad (-45 < A < -3, \quad k = 0.048).$$

The parameter A is defined as

$$A = \left(\frac{\rho_p}{\rho_g} - 1\right) M_A, \quad M_A = \frac{d}{U_r^2}\frac{\mathrm{d}U_r}{\mathrm{d}t}, \tag{3}$$

where U_r is the relative velocity between fluid and droplet. For the decelerating motion of the droplets in the experiments the derivative $\mathrm{d}U_r/\mathrm{d}t$ is the negative quantity. Hence we can use the formula (3) to estimate the difference between unsteady and steady drag coefficients. The parameter A in our problem decreases in time from the value $A = -1.6$. Corresponding deviation of the steady drag coefficients from the unsteady one calculated by (3) is less than 1%. It allows us to conclude that the change of drag coefficient caused by unsteadiness can be neglected.

The Basset force expressed by the integral term in (1) is due to combined action of viscosity and (mostly) acceleration. It has a drag effect on the particle in unsteady motion. In most works on aerosol particle motion the Basset force is usually neglected due to small influence and numerical difficulties. Fuchs (1964) noted the importance of the Basset force for decelerating motion of particles. It leads to an increase of stopping distance of decelerating particles.

Note that the expression for the Basset force in (1) is not fully consistent with the Navier–Stokes Equation (NSE) since the droplet drag law in (1) differs from the linear Stokes law whereas the Basset term stems from the time-dependent linearized solution (Landau and Lifshitz, 1995). Lovalenti and Brady (1993) pointed out that the history force for a sphere

with Reynolds correction undergoing step velocity changes behaves as t^{-2} during acceleration from rest and as t^{-1} when it comes to rest whereas for changes between finite velocities the history force decays exponentially. Furthermore, Lawrence and Weinbaum (1986) have shown that the history force also depends on particle shape introducing still another additional temporal behavior.

Experimentally, Mordant and Pinton (2000) for macroscopic solid spheres starting from rest in water observed for short times $t^{-1/2}$ behavior while at long times history force was better fitted by exponential decay. In view of the short observation times in our experiments and the unsettled questions concerning the true behavior of the history force mentioned above we used the Eq. (1) with Basset force in the form as in the most previous works. Such Basset term yields a $t^{-1/2}$ dependence on time. To take into account finite particle Reynolds numbers a correction coefficient C_h is applied to the history term in Eq. (1) (Kim et al., 1998).

Accordingly Odar and Hamilton (1964), the coefficient can be expressed for $Re_p < 60$ as

$$C_h = 0.48 + 0.52M_A^3/(1 + M_A)^3.$$

Finally we should note that the Basset force for particles in a chain differs from the isolated particle case. But we used in (1) the expression for the Basset force as for a single droplet. This assumption is based on the conclusion of the theoretical work of Leichtberg et al. (1976) that the Basset force in a configuration only slowly changes due to particle interaction. This conclusion was made for the multiparticle gravitational-Stokes flow interactions. It is reasonable that this conclusion is valid for our case.

To account for the particle drag reduction due to the influence of neighboring particles in a particle chain an interaction parameter λ is introduced, defined as the ratio of the drag coefficient of a particle in a chain, C_D to the one of an isolated single particle, C_{D0}, i.e. $\lambda = C_D/C_{D0}$. The introduced interaction parameter expresses the drag correction of the single droplet due to the interaction with other droplets. In general for the two-dimensional droplet travel path observed in experiments λ is a function of all the particle spacing and velocities and their spatial arrangement relative to each other. From the results of previous works on the particle interaction in linear chain it can be concluded that the nearest leading particle has the largest influence on a trailing particle's drag when they move along the common axis. Therefore, as mentioned above, the radius of curvature of the droplet trajectory is much larger than its size. Because of this, it is justified to assume that the interaction parameter depends only on the distance s between two interacting droplets $\lambda = \lambda(s)$, and data for drag correction due to the hydrodynamic interaction in the fluid flow past the linear array of the solid spheres can be used.

The aerosol droplets observed in experiments move practically by the same trajectory without considerable oscillations (Figs. 3 and 4). Then to calculate the particle motion in a chain we adopt the approach used in the work of Ruzicka (2000) for motion of bubbles with all particles being identical. Such a model describes the behavior of particles in a stable chain that is actually observed. We consider all droplets as the trailing particles and use the Eq. (1) for description their travel by the same trajectory. Instabilities and neutral oscillations would make this approach unsuitable. Including the interaction parameter $\lambda = \lambda(s)$ into a modified relaxation time τ^*, the equations of particle motion in a Cartesian coordinate system taking into account (2) can be written in the form

$$\begin{aligned}
\frac{dv_x}{dt} &= -\frac{v_x}{\tau^*}(1+\psi v^{0.687}) - b\int_0^t \frac{dv_x}{d\tau}\frac{d\tau}{\sqrt{t-\tau}},\\
\frac{dv_y}{dt} &= -\frac{v_y}{\tau^*}(1+\psi v^{0.687}) - g - b\int_0^t \frac{dv_y}{d\tau}\frac{d\tau}{\sqrt{t-\tau}},\\
\frac{dx}{dt} &= v_x, \quad \frac{dy}{dt} = v_y,
\end{aligned} \tag{4}$$

where v_x, v_y are the particle velocity components, $\tau^* = \tau_{St}/\lambda(s)$ is the Stokes particle relaxation time $\tau_{St} = \rho_p d^2/18\mu$ modified by the hydrodynamic interaction parameter λ with the other droplets in the chain, ρ_p is the particle density, g is the gravity acceleration,

$$\psi = 0.15(d\rho_g/\mu)^{0.687}, \quad v = \sqrt{v_x^2 + v_y^2}, \quad b = 9C_h\sqrt{\mu\rho_g}/d\rho_p\sqrt{\pi}.$$

The non-dimensional inter-particle distance s (defined as the shortest distance between the droplets surfaces divided by the particle diameter d) for a given motion law of chain particle $x = x(t)$, $y = y(t)$ can be written as (for 2D motion)

$$s = \frac{\sqrt{(x(t+t_g)-x(t))^2 + (y(t+t_g)-y(t))^2}}{d} - 1. \tag{5}$$

$t_g = 1/v_g$ is the particle generation time interval (v_g is the generation rate).

The initial conditions in (4) at $t = 0$ take the form

$$v_x = -v_0, \quad v_y = 0, \quad x = 0, \quad y = 0 \tag{6}$$

for horizontal motion and

$$v_x = 0,\ v_y = v_0,\ x = 0,\ y = 0 \tag{7}$$

for vertical motion.

To close the system (4) we should determine the function $\lambda = \lambda(s)$. There is little information in the literature concerning the drag correction function for finite small Reynolds numbers in unsteady chains. As first approximation the assumption is reasonable that the main part of drag reduction of particle in a chain in the small Reynolds number region can be obtained by means of the creeping flow theory. Because of this, neglecting the complexity of the drag in an unsteady chain of many interacting droplets, we used instead the data from a theory for stationary Stokes flow of a linear array of spheres at fixed distances based on the multipole representation technique (Gluckman et al., 1971). Within this theory the magnitude of the hydrodynamic interaction between droplets grows with increasing chain length and decreasing droplet distance. The results of Gluckman et al. also show that the relative change of the drag reduction strongly decreases starting with chains consisting of more than a few spheres. We used the theoretical values of the drag reduction according to the results for the middle sphere in chains of 7 and 101 spheres at different spacing distances. The fitting functions for the respective data as a function of the no dimensional inter-particle distance s are

$$\lambda = 1 - \exp(-0.32\text{–}0.16\,s) \quad (n = 7) \tag{8}$$

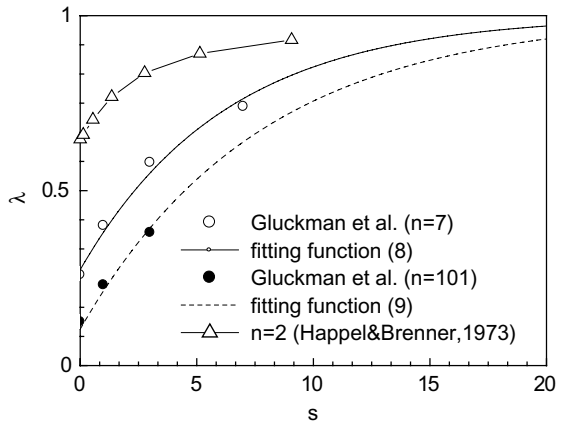

Fig. 5. The drag correction as a function of inter-particle distance.

$$\lambda = 1 - \exp(-0.11\text{–}0.13\,s) \quad (n = 101) \tag{9}$$

where n is the number of spheres in a chain. Fig. 5 shows the $\lambda = \lambda(s)$ according to the above relations (8) and (9) together with Gluckman's data. The upper curve in the graph corresponds to the drag reduction function for two particles moving along a line connecting their centers in creeping flow (Happel and Brenner, 1973). As expected, the drag correction function for a chain of many particles is lower than for only two particles. Comparing the $\lambda(s)$ for two interacting droplets in Stokes flow with experimental data for $Re > 0$ from different authors shows that the curve of Happel and Brenner (1973) can be taken as bounding curve $\lambda(s)$. Therefore, we can conclude that for finite Reynolds numbers $\lambda(s)$ should be located somewhat lower than the functions (8) and (9).

Employing (4), (8) and (9) we will consider the interaction parameter $\lambda(s(t))$ as a function of time. To find the function $s(t)$ and therefore $\lambda(t)$ a simple iteration procedure was used. Equations (4) are solved numerically many times starting with $\lambda = 1$. The numerical function $s(t)$ from previous iteration is used by interpolation to express the function $\lambda(t)$ on the each next iteration. A few iterations will suffice to obtain a converging solution.

In order to roughly assess the importance of the history term (4) was solved with and without it.

4. Results and discussion

For comparing theory with experiment, the droplets were photographed and average values of λ_0 for whole chains (produced with different droplet generation intervals t_g) were determined by least square fitting to the droplet locations. The values of λ_0 for horizontal and vertical jets of droplets at the same generation rate are very close and the fit to the experiments resulted in

$$\lambda_0 = 1 - \exp(0.56 - 1.74\, t_g^{0.56}). \tag{10}$$

(t_g in ms). This was done by numerically solving (4) for the interaction parameter λ_0 for all the different generation time intervals t_g.

For a simple display of the results we investigated the droplet trajectory endpoints x_s for horizontal jets and the height of particle vertical jump y_s for vertical jets. The quantity x_s is defined as the distance in horizontal direction traveled by a droplet until it leaves the lower frame boundary, i.e. after having fallen ~1 cm vertically downward. The parameter y_s for vertical motion is determined as the distance of upward droplet motion until the vertical velocity reverses sign.

In general, the Basset force integral should include the sudden change of particle velocity up to the initial velocity v_0 and subsequent deceleration (Landau and Lifshitz, 1995). Part of Basset integral connected with initial sudden acceleration can be written after integration in an analytical form

$$J_0 = v_0 b \frac{1}{\sqrt{t}}.$$

A globally adaptive scheme based on Gauss–Kronrod rules (Calvetti et al., 2000) was used to calculate the integral in the expression for the historical force with the velocity derivative due to the particle deceleration.

Some results of the numerical calculations are presented in the Figs. 6–10. Note that these results were obtained by numerical integration the Basset force term without accounting for the initial acceleration. Fig. 6 shows the droplet trajectory endpoints with and without Basset force influence as a function of t_g according to the above-described numerical model using the theory-based variables $\lambda(s)$ (8) and (9) and λ_0 derived from experiments in the form (10). As t_g decreases, the trajectory endpoint grows due to increasing particle interactions in the droplet chain. The theoretical curve of the dependence $x_s(t_g)$ obtained by solving (4) with the drag reduction law for a chain with 101 particles is higher than the corresponding curve for $n = 7$ due to the

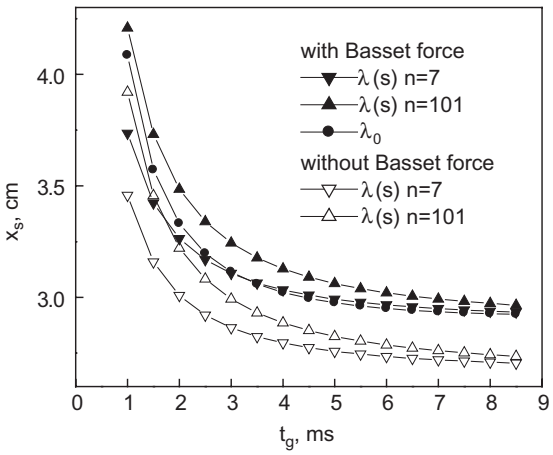

Fig. 6. Comparison of the dependence of the droplet trajectory endpoints on the particle generation time interval t_g for horizontal jet. Numerical model: open and filled triangles are the results of calculation without and with Basset force influence. Experimental trajectories: filled circles.

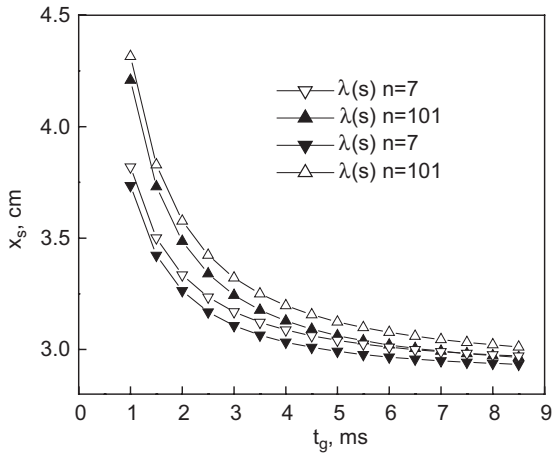

Fig. 7. Comparison of the dependence of the theoretical droplet trajectory endpoints on the particle generation time interval t_g for the horizontal jet obtained from numerical integration Basset force integral (full marks) and using approximate formula (11) (open marks).

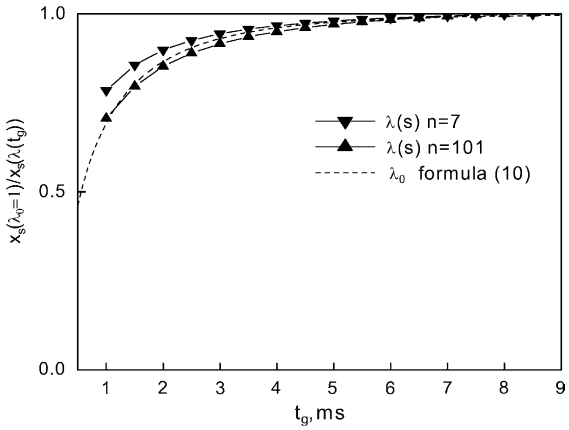

Fig. 8. The relative droplet trajectory endpoint for horizontal jet as a function of the particle generation time interval t_g.

larger drag reduction of a center particle in a longer chain. The experimental curve for λ_0 lies between the numerical curves obtained at $n = 7$ and $n = 101$, respectively. This makes sense, since the observable part of the chain changes from ten particles for $t_g = 8$ ms to almost one hundred particles for $t_g = 1$ ms. The fair agreement between the numerical approach and experimental data means also that the resistance reduction in creeping flow can be applied in combination with the Reynolds correction.

For decelerating particles the Basset force increases the droplet trajectory endpoint as can be seen from the Fig. 6. The theoretical curves $x_s(t_g)$ calculated without Basset force lie below the

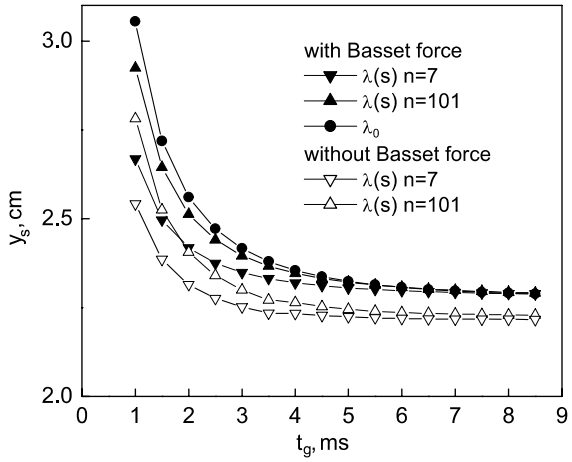

Fig. 9. Comparison of the dependence of the height of the droplet vertical jump on the particle generation time interval for vertical jet. Numerical model: open and filled triangles are the results of calculation without and with Basset force. Experimental trajectories: filled circles.

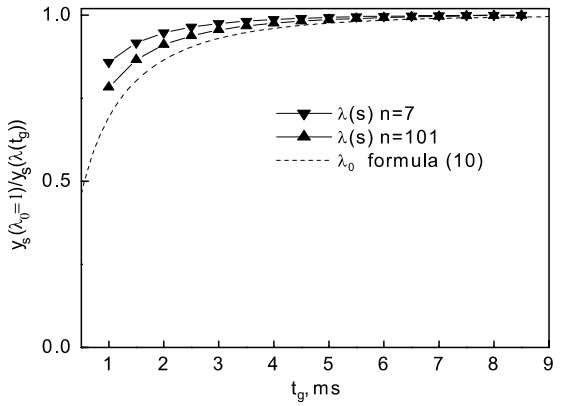

Fig. 10. The relative height of particle vertical jump as a function of the particle generation time interval t_g.

corresponding curves obtained including Basset force term because the influence of history (Basset) force on the interacting droplets motion partly compensates for the Reynolds correction in our experimental conditions.

The numerical integration in the Basset force term is a time consuming procedure. Because of this, we checked also the simple approximation for the Basset integral given in Nigmatulin (1990). According to Nigmatulin we can approximately express the history force integral as

$$\int_0^t \frac{\mathrm{d}v}{\mathrm{d}\tau}\frac{\mathrm{d}\tau}{\sqrt{t-\tau}} \approx \frac{v-v_0}{\sqrt{0.5t}}. \tag{11}$$

Formula (11) is the expression of the mean value theorem for definite integral choosing $\tau = 0.5t$ as an average value. The dependencies of droplet trajectory endpoints on t_g calculated by numerical integration of the history force term and approximate formula (11) shown in Fig. 7. The small difference between the results obtained by means of two approaches (no greater than 3%) indicates that the simple formula (11) works well and can be used to express the history force integral in non-stationary problems.

It should be noted also that accounting the initial droplet acceleration during nozzle ejection reduces the Basset force term in disagreement with observation. We believe this could be due to the liquid jet oscillations back into and out of the nozzle and the gas flow boundary conditions there.

The fit to the experiments λ_0 is shown together with the ratio $x_s(\lambda_0 = 1)/x_s(\lambda(t_g))$ for horizontal jets in Fig. 8. Obviously, the ratio for $n = 101$ almost coincides with the experimental function $\lambda_0(t_g)$.

Figs. 9 and 10 show similar data for vertical motion, i.e. including the effects of gravitational deceleration from the numerical solution of (4) and (7) with and without the Basset force. The same conclusions as above can be drawn for vertical motion, too. The theoretical model predicts a slightly larger interaction parameter than for horizontal motion case i.e. a smaller hydrodynamic interaction. This can be explained by the absence of additional forces and particle collisions in the theoretical model. Actually, in experiments pairing and particle collisions were observed for vertical jet, respectively. Such effects will have to be addressed in future studies.

5. Conclusions

Experiments demonstrate a noticeable hydrodynamic interaction between moving droplets in a horizontal and vertical chains resulting in increased distances traveled by droplets for otherwise unchanged diameters and initial velocities.

Applying a stationary interaction model within creeping flow approximation and combining it with the standard history force, we find reasonable agreement of experimental results with the solution of the equation of droplet motion including the drag correction of the droplets in chain.

Acknowledgments

This work was supported by the German Academic Exchange Service DAAD (N 325-2002) and partially by Russian Foundation for Basic Research under grant number 02-01-00836 as well as by German Space Agency DLR under grant 50WM0037.

References

Calvetti, D., Golub, G.H., Gragg, W.B., Reichel, L., 2000. Computation of Gauss–Kronrod quadrature rules. Math. Comput. 69, 1035–1052.

Chen, R.C., Lu, Y.N., 1999. The flow characteristics of an interactive particle at low Reynolds numbers. Int. J. Multiphase Flow 25, 1645–1655.
Chen, R.C., Wu, J.L., 2000. The flow characteristics between two interactive spheres. Chem. Eng. Sci. 55, 1143–1158.
Chiang, C.H., Sirignano, W.A., 1993a. Axisymmetric calculations of three-droplet interactions. Atomization Sprays 3, 91–107.
Chiang, C.H., Sirignano, W.A., 1993b. Interacting, convecting, vaporizing fuel droplets with variable properties. Int. J. Heat Mass Transfer 36, 875–886.
Clift, R., Grace, J.R., Weber, M.E., 1978. Bubbles, Drops and Particles. Academic Press, New York.
Fuchs, N.A., 1964. The Mechanics of Aerosols. Pergamon Press, Oxford.
Gluckman, J., Pfeffer, R., Weinbaum, S., 1971. A new technique for treating multiparticle slow viscous flow: axisymmetric flow past spheres and spheroids. J. Fluid Mech. 50, 705–740.
Happel, J., Brenner, H., 1973. Low Reynolds Number Hydrodynamics. Noordhoff Int. Publishing, ISBN 90 01 37115 9.
Kim, I., Elghobashi, S., Sirignano, A., 1993. Three-dimensional flow over two spheres placed side by side. J. Fluid Mech. 246, 465–488.
Kim, I., Elghobashi, S., Sirignano, A., 1998. On the equation for spherical-particle motion effect of Reynolds number and acceleration numbers. J. Fluids Mech. 367, 221–253.
Landau, L.D., Lifshitz, E.M., 1995. Fluid Mechanics, second ed.Course of Theoretical Physics, vol. 6 Pergamon.
Lavergne, G., Adam, O., Virepinte, J.E., Biscos, Y., 1997. An experimental study on droplet interaction. Int. J. Fluids Mech. Res. 24, 450–460.
Lawrence, C.J., Weinbaum, S., 1986. The force on an axisymmetric body in linearized, time-dependent motion: a new memory term. J. Fluid Mech. 171, 209–218.
Lee, K.C., 1979. Aerodynamic interaction between two spheres at Reynolds numbers around 10^4. Aeronaut.Q. 30, 371–385.
Leichtberg, S., Weinbaum, S., Pfeffer, R., Gluckman, M.J., 1976. A study of unsteady forces at low Reynolds number: a strong interaction theory for the coaxial settling of three or more spheres. Philos. Trans. Roy. Soc. A 282, 585–610.
Liang, S.C., Hong, T., Fan, L.S., 1996. Effect of particle arrangements on the drag force of a particle in the intermediate flow regime. Int. J. Multiphase Flow 22, 285–306.
Lovalenti, P.M., Brady, J.F., 1993. The hydrodynamic force on a rigid particle undergoing arbitrary time-dependent motion at small Reynolds number. J. Fluid Mech. 256, 561–605.
Maxey, M.R., Riley, J.J., 1983. Equation of motion of a small rigid sphere in a nonuniform flow. Phys. Fluids 26, 883.
Michaelides, E.E., 1997. Review—the transient equation of motion for particles, bubbles and droplets. J. Fluids Eng. 119, 233–247.
Mordant, N., Pinton, J.F., 2000. Velocity measurement of a settling sphere. Eur. Phys. J. B 18, 343–352.
Mulholland, J.A., Srivastava, R.K., Wendt, J.O.L., 1988. Influence of droplets spacing on drag coefficient in nonevaporating, monodisperse streams. AIAA J. 26, 1231–1237.
Nguen, Q.V., Dunn-Rankin, D., 1992. Experiments examining drag in linear droplets packets. Exp. Fluids 12, 157–165.
Nguen, Q.V., Rangel, R.H., Dunn-Rankin, D., 1991. Measurement and prediction of trajectories and collision of droplets. Int. J. Multiphase Flow 17, 159–177.
Nigmatulin, R.I., 1990Dynamics of Multiphase Media, vol. 1. Hemisphere, New York.
Odar, F., Hamilton, W.S., 1964. Forces on a sphere in a viscous fluid. J. Fluid. Mech. 18, 302–314.
Raju, M.S., Sirignano, W.A., 1990. Interaction between two vaporizing droplets in an intermediate Reynolds number flow. Phys. Fluids A 2, 1780–1796.
Rowe, P.N., Henwood, G.A., 1961. Drag forces in a hydraulic model of a fluidised bed—Part 1. Trans. Inst. Chem. Eng. 39, 43–54.
Ruzicka, M.C., 2000. On bubbles rising in line. Int. J. Multiphase Flow 26, 1141–1181.
Tal, R., Lee, D.N., Sirignano, W.A., 1983. Hydrodynamics and heat transfer in sphere assemblages—cylindrical cell models. Int. J. Multiphase Flow 26, 1265–1273.
Temkin, S., Mehta, H.K., 1982. Droplet drag in an accelerating and decelerating flow. J. Fluid Mech. 116, 297–313.
Tsai, J.S., Sterling, A.M., 1990. The application of an embedded grid to the solution of heat and momentum transfer for spheres in a linear array. Int. J. Heat Mass Transfer 33, 2491–2502.

Tsuji, Y., Morikawa, Y., Terashima, K., 1982. Fluid–dynamic interaction between two spheres. Int. J. Multiphase Flow 8, 71–82.

Zhu, C., Liang, S.C., Fan, L.S., 1994. Particle wake effects on the drag force of interactive particle. Int. J. Multiphase Flow 20, 117–129.